Electronic Supplementary Information (ESI) for: "Cm^{3+}/ Eu^{3+} Induced Structural, Mechanistic and Functional Implications for Calmodulin"

Björn Drobot, Moritz Schmidt, Yuji Mochizuki, Takaya Abe, Koji Okuwaki, Florian Brulfert, Sven Falke, Sergey A. Samsonov, Yuto Komeiji, Christian Betzel, Thorsten Stumpf, Johannes Raff, and Satoru Tsushima

Table of Content

1 Materials and Methods

1.1 CaM purification.

CaM was purified as previously described[1] with minor modifications. After the initial purification using affinity chromatography with a phenyl sepharose column CaM was lyophilized for storage. Prior to each experiment CaM (~20 mg·m^{-1}) was resolved in 6 M guanidine hydrochloride plus 200 mM EDTA, after which it was transferred to 100 mM NaCl using a desalting column (sephadex G50). The protein concentration was determined via UV-absorbance (E = 2980 M^{-1}cm^{-1}).

1.2 Sample preparation for isothermal titration calorimetry (ITC).

For Eu^{3+} binding via ITC, the cell CaM concentration was adjusted to 60 μM and titrated with 2 mM $EuCl_3$. Both solutions were pre-adjusted to pH 4.5 using HCl.

For the enzymatic assay all samples were prepared in a HEPES (50 mM) and NaCl (100 mM) buffer. The concentration of PDE (2 nM), CaM (160 nM) was constant in all samples. To determine calcium-induced activity, a concentration of 10 μM was used. Eu^{3+} activation was studied at a concentration of 800 nM. All solutions were preadjusted to pH 7.4 and ITC assays were performed at $30\,^{\circ}\mathrm{C}$. A cAMP (Sigma Aldrich) solution of 5 mM was used for the multiple-injection method.

1.3 ITC experimental setup.

In order to investigate the thermodynamics of Eu^{3+} ion binding to CaM, binding affinity was studied using ITC (MicroCal, Malvern Instruments). The heat flow of 39 injections in 1 μl steps into a 203.6 μl cell at $25\,^{\circ}\mathrm{C}$ was recorded with a 1 s time resolution. A titration of 2 mM $EuCl_3$ to 100 mM NaCl was used as background. Individual injections were integrated followed by background subtraction. These data were analyzed using a model with four different Eu^{3+}-CaM complexes, based on the four EF-hands of CaM. This experiment was replicated (Figure S5 and S6).

Enzymatic activity was also investigated via ITC (Nano ITC, TA Instruments) Specifically, enzyme kinetics were determined using the multiple injection method which derives the enzymatic activity from the heat flow produced by the reaction. Reaction cells (1 mL) were filled and equilibrated at the indicated temperature. 40 injections of a 5 mM cAMP solution were made every 240 s at a stirring speed of 250 rpm; thermal power was than recorded every second. The measured thermal power generated by the enzyme enables on to calculate the reaction rate (Eq. 2). The observed heat flow (μJ s^{-1}) is proportional to the reaction rate. To determine the reaction rate, both the enthalpy of the reaction (ΔHr) of interest and the cell volume (V) have to be known.

$$\Delta Hr = \frac{1}{n_{sub}} \int_{t=0}^{t=\infty} \frac{dQ}{dt} dt \tag{1}$$

where n_{sub} is the number of moles of catalyzed substrate and dQ/dt is the generated power. The reaction rate can then be calculated as follows

$$Rate = \frac{1}{V \cdot \Delta Hr} \frac{dQ}{dt} \tag{2}$$

using the ITC cell volume V (1 ml): Additional details about the equation and the method used herein can be found in the literature.[2,3]

1.4 Sample preparation for Time-Resolved Laser-induced Fluorescence Spectroscopy (TRLFS).

An initial series of Eu^{3+}-CaM TRLFS (Fig. 2) was carried out either by titrating $EuCl_3$ solution to a CaM solution or vice versa. All solutions were pre-adjusted to pH 4.5 using HCl to avoid Eu^{3+} hydrolysis. For the titration of Eu^{3+} to CaM, both solutions contained 8.4 μM CaM to prevent dilution. In comparison, for the titration of CaM to Eu^{3+}, both solutions contained 10 μM $EuCl_3$. The desired concentrations were tuned by adding the appropriate titrant volume to the sample solution. After analyzing data via PARAFAC, the complex distribution was fitted to the Hill equation.

$$I([\mathrm{Eu}^{3+}]) = \frac{I_{max} \cdot [\mathrm{Eu}^{3+}]^n}{k^n \cdot [\mathrm{Eu}^{3+}]^n} \tag{3}$$

Where [Eu] is the total Eu^{3+} concentration, I_{max} is the limiting intensity at infinite [Eu], k is the [Eu] giving $I_{max}/2$, and n is a shaping factor for the sigmoidal character.

For the second Eu^{3+}-CaM TRLFS series (Fig. S2), 6 samples containing 10^{-5} M $EuCl_3$ and varying concentrations of CaM (10^{-7} to 2.5·106−6) were prepared by mixing a 10^{-5} M $EuCl_3$ solution with CaM stock solutions (both pH 4.5) to achieve desired CaM concentrations. Note, that the CaM stock solution contained the same amount of $EuCl_3$ to avoid Eu^{3+} dilution. Using a similar approach, the $CaCl_2$ concentrations were adjusted for the second part of the series. Specifically the $CaCl_2$ stock solution (pH 4.5) contained an additional 10^{-5} M $EuCl_3$ and 2.5·106−6 CaM.

The third Eu^{3+}-CaM TRLFS series (Fig. 3) was prepared as previously described. Thus, a total of 29 samples with a fixed 10^{-5} M $EuCl_3$ concentration was mixed with the CaM stock solution containing 10^{-5} M $EuCl_3$. All solutions were preadjusted to pH 4.5.

Using Cm^{3+} as a fluorescent probe facilitates studying the system at at significantly lower metal ion concentrations. Accordingly, we prepared a pH series at constant $[Cm^{3+}] = 100$ nM and constant [CaM] over the pH range of 3.1 - 9.0. The low metal ion concentration requires several precautions to prevent unwanted competition reactions – both, with other metal cations, e.g. Na^+, as well as impurities of other complexation ligands. After purification, [CaM] was adjusted to 10 μM in 0.1 M KCl as a background electrolyte. KCl was chosen due to the relatively larger ionic radius of K^+ compared to Na^+ and Ca^{2+}. The latter feature very similar ionic radii (rVI(Na^+ = 1.02 Å, rVI(Ca^{2+}) = 1.00 Å[4]), which permit facile exchange of the two ions in the binding site of CaM.[5] The larger K^+ ions (rVI(K^+) = 1.38 Å[4]) do not easily fit the cation binding site of the protein and can be assumed to be inert in the complexation reaction. Finally, pH was adjusted to 3.0 ± 0.1 using $HClO_4$ and KOH, and $[Cm^{3+}]$ was added to yield a concentration of $[Cm^{3+}] = 100$ nM. The number of coordinating water molecules of Cm^{3+} was determined according to Kimura's equation.[6]

$$n_{H_2O} = 0.65 \cdot \frac{1}{\tau} - 0.88 \tag{4}$$

Here τ represents the lifetime in ms.

1.5 TRLFS experimental setup.

For time-resolved laser-induced fluorescence measurements of Eu^{3+}, we selected an excitation wavelength of 394 nm (Laser: Quantaray Lab 170-20, Spectra-Physics; OPO: flexiScan, GWU-Lasertechnik Vertriebsges.mbH). After passing through the spectrometer (MS257 Modell 77700A, Oriel Instruments, Gitter: 300 lines mm^{-1}), the emitted light was detected by an ICCD camera (iStar DH720-18H-13, Andor Technology) with an initial delay of 10 μs and a step width of 15 μs. Data were analyzed using PARAFAC as described previously.[7–9] The luminescence of Cm^{3+} was excited using a pulsed (20 Hz) XeCl-excimer laser (Lambda Physics, EMG, 308 nm) pumped dye laser (Lambda Scanmate) with QUI as lasing dye tuned to the resonance wavelength of Cm^{3+}'s $^8S_{7/2}$ (Z) $\rightarrow$ $^6D_{7/2}$ (A) transition at 396.6 nm. Luminescence was recorded by an optical multichannel analyzer that consists of a polychromator with 300, 600, and 1200 lines mm^{-1} gratings (Jobin Yvon) and a gated photodiode array detector (Spectroscopy Instruments) cooled to $-20\,^{\circ}C$ for an improved signal-to-noise ratio. The grating was calibrated by the emission lines of a neon lamp for each measurement. In order to record luminescence lifetimes, the delay time between the laser pulse and the start of the measurement was varied from 10 to 660 μs.

1.6 Monte Carlo for error estimation.

ITC and TRLFS data were analyzed optimizing the speciation of Eu(III) and CaM. For both methods curve fitting was performed that featured optimization of multiple parameters. In order to estimate the robustness of the fitted parameters, a Monte Carlo approach was employed. Random noise of the order of the best fit residuals was added to the raw data. At least 200 of these datasets were generated and analyzed. The distribution of the extracted parameters were used for the parameter-error estimation provided in the manuscript. The results of the Monte Carlo runs are summarized in Figure S2 (TRLFS) and Figure S3 and S5 (ITC).

2 Computational details

2.1 Molecular Dynamics (MD) simulations.

MD simulations and data analyses were performed using AMBER 14 program package[10] with ff99SB force field applied on the protein. For Ca^{2+},[11] Eu^{3+},[12] and Cm^{3+}[13] ions, additional parameters were employed. The starting structure of holo-CaM was obtained from a prior literature report.[14] Since there are four missing residues in the XRD structure, these residues were manually added; conversely, the oxygens of the hydration waters were removed. Finally, the protonation state of the protein was adjusted using the MOE v2015.10 program (Chemical Computing Group Inc.) to model physiological pH. In the case of Eu^{3+} and Cm^{3+} bound CaM, all four Ca^{2+} ions were replaced by these ions. Note that 16 Na^+ ions for Ca^{2+}-CaM, and 12 Na+ ions for Eu^{3+}-CaM and Cm^{3+}-CaM were added to make the system electrostatically neutral. Then, TIP3P waters were added with a minimum water layer thickness of 8 Å. 500 steps of steepest decent and 500 steps of conjugate gradient – with 500 kcal·mol^{-1}·Å^{-1} harmonic restraint on the protein – was initially conducted, after which 1000 steps of steepest decent and 1500 steps of conjugate gradient were performed without constraints. 40 ps of heating of the system from 0 to 300 K with 10 kcal·mol^{-1}·Å^{-1} harmonic restraint on the protein,

after which another 1 ns preconditioning run was performed at 300 K without restraint on the solutes. Finally, a 100 ns MD simulation run was performed in a periodic boundary condition in an NPT ensemble.[15] Simulations were terminated and restarted every 5 ns. The SHAKE algorithm, a 2 fs time integration step, 12 Å cutoff for non-bonded interactions, and the particle mesh Ewald (PME) method were used. MD trajectory was recorded at every 50 ps. Oxygen atoms within 2.7 Å distance from metal centers were defined as coordinated atoms.

2.2 Fragment molecular orbital (FMO) calculations.

FMO calculations were performed on Ca^{2+}-CaM and Eu^{3+}-CaM. The input structures were constructed from MD trajectories by taking snapshots (each 1 ns) of each of the simulations (100 ns). The resulting 100 structures (for each of Ca^{2+}-CaM and Eu^{3+}-CaM) consist of over 30,000 atoms; as such, the total number was too large for FMO input. Since most hydration waters play a marginal role in metal–protein interactions, all hydration waters – except those within 4 Å from the protein surface – were stripped off.[16] The final FMO input molecules consisted of (1) CaM, (2) 4 metal cations (Ca^{2+} or Eu^{3+}), (3) 12 (for Eu^{3+}-CaM) or 16 (for Ca^{2+}-CaM) Na^{+} ions, and (4) 672 - 692 waters. The total number of atoms was roughly 4300 for each input file. Each amino acid residue was treated as single fragment and the whole molecule was fragmentated into 148 amino acid residues, 4 metal ions, 12 or 16 Na^{+} ions, and waters. The inter-fragment interaction energy (IFIE)[17] was used to analyze the interactions between metal centers (Ca^{2+} and Eu^{3+}) and surrounding amino acid residues, as well as those amongst the residues. To reduce overestimation in IFIEs for electrostatic-dominant cation-residue interactions, a decay factor of exp(-0.3R)/R was introduced (Yukawa potential, R is the distance between ion and residue). Note that we were unable to calculate the Cm^{3+}-CaM at the FMO/MP2 level as f orbitals are still not implemented in the ABINIT-MP program.

3 Additional tables and figures

Table S1: Average coordination number (defined as O atoms within 2.7Å from the metal) around the metal ions in Ca^{2+}, Eu^{3+}, and Cm^{3+} bound CaM during 100 ns MD simulation and their comparison with crystal structure of holo–CaM. Non-coordinating residues are omitted for simplicity.

EF hand 1

res	type	Ca_{cr} [b]	Ca	Eu	Cm
21	ASP	1	1.00	1.06	1.00
23	ASP	1	1.03	1.49	1.53
25	ASP	1	1.00	1.93	1.96
27	THR	1	1.00	0.95	0.88
32	GLU	2	1.98	2.00	2.00
water		1	1.00	1.68	1.81
total		7	7.01	9.11	9.17

EF hand 2

res	type	Ca_{cr} [b]	Ca	Eu	Cm
57	ASP	1	1.00	1.00	1.00
59	ASP	1	1.11	1.28	1.28
61	ASN	1	1.00	0.98	0.98
63	THR	1	0.98	0.77	0.81
65	ASP	0	1.02	1.08	1.28
68	GLU	2	1.98	1.99	1.98
water		1	0.01	1.83	1.65
total		7	7.10	8.93	8.97

EF hand 3

res	type	Ca_{cr} [b]	Ca	Eu	Cm
94	ASP	1	1.00	1.00	1.00
96	ASP	1	1.43	1.87	1.89
98	TYR	1	1.00	1.00	0.98
100	THR	1	1.00	0.27	0.60
105	GLU	2	1.99	1.99	1.99
water		1	1.00	2.86	2.77
total		7	7.41	8.99	9.23

EF hand 4

res	type	Ca_{cr} [b]	Ca	Eu	Cm
130	ASP	1	1.00	1.00	1.77
132	ASP	1	1.03	1.13	1.82
134	ASP	1	1.00	1.99	1.96
136	GLN	1	1.00	0.97	0.92
141	GLU	2	1.99	2.00	1.99
water		1	1.00	1.99	1.18
total		7	7.01	8.99	9.63

[b] from crystal structure of Ca^{2+}–CaM

Table S2: Average inter-fragment interaction energy (IFIE, in kcal·mol^{-1}) between metal centers and surrounding residues in Ca^{2+}-CaM and in Eu^{3+}-CaM calculated by fragment molecular orbital (FMO) method at the MP2/6-31G* level from 100 MD snapshots and their standard deviations.

		EF hand 1				EF hand 2	
res	type	Ca^{2+}	Eu^{3+}	res	type	Ca^{2+}	Eu^{3+}
21	ASP	-61.5 ± 3.8	-91.6 ± 6.0	57	ASP	-62.3 ± 3.6	-88.6 ± 5.3
22	LYS	+5.3 ± 1.6	6.4 ± 2.0	58	ALA	2.0 ± 1.2	1.2 ± 0.7
23	ASP	-53.6 ± 4.2	-86.7 ± 10.3	59	ASP	-52.8 ± 4.3	-82.1 ± 7.8
24	GLY	+1.6 ± 0.6	1.3 ± 0.5	60	GLY	1.8 ± 0.6	1.4 ± 0.4
25	ASP	-50.3 ± 3.5	-92.9 ± 5.9	61	ASN	-9.6 ± 2.1	-18.0 ± 2.8
26	GLY	+1.9 ± 0.5	2.0 ± 0.5	62	GLY	1.5 ± 0.4	1.8 ± 0.4
27	THR	+2.9 ± 0.8	1.9 ± 1.1	63	THR	2.3 ± 0.9	1.0 ± 0.9
28	ILE	-22.7 ± 2.4	-33.1 ± 5.2	64	ILE	-19.9 ± 2.8	-28.0 ± 5.0
29	THR	+3.2 ± 0.8	3.3 ± 1.0	65	ASP	-48.3 ± 3.4	-71.3 ± 6.6
30	THR	+0.4 ± 0.1	0.5 ± 0.2	66	PHE	1.2 ± 0.2	1.4 ± 0.2
31	LYS	+1.0 ± 0.4	1.3 ± 0.5	67	PRO	0.1 ± 0.0	0.2 ± 0.1
32	GLU	-63.6 ± 3.5	-99.1 ± 4.1	68	GLU	-65.1 ± 3.6	-95.9 ± 4.8
water		-9.7 ± 1.3	-25.9 ± 2.1	water			-29.3 ± 2.0
Total		-245.0 ± 8.3	-412.6 ± 15.3	Total		-249.0 ± 8.4	-406.2 ± 14.0

		EF hand 3				EF hand 4	
res	type	Ca^{2+}	Eu^{3+}	res	type	Ca^{2+}	Eu^{3+}
94	ASP	-62.4 ± 4.0	-91.4 ± 6.7	130	ASP	-62.5 ± 3.4	-90.6 ± 5.3
95	LYS	5.5 ± 1.3	6.4 ± 1.2	131	ILE	2.5 ± 1.0	2.4 ± 1.1
96	ASP	-56.8 ± 4.6	-89.9 ± 5.7	132	ASP	-53.0 ± 3.8	-79.3 ± 8.1
97	GLY	1.7 ± 0.6	1.4 ± 0.4	133	GLY	1.9 ± 0.7	1.1 ± 0.5
98	TYR	-10.0 ± 2.0	-19.1 ± 2.9	134	ASP	-50.8 ± 3.1	-92.2 ± 4.7
99	GLY	1.6 ± 0.3	1.7 ± 0.4	135	GLY	1.5 ± 0.4	1.8 ± 0.4
100	THR	2.4 ± 0.6	1.7 ± 0.6	136	GLN	3.8 ± 0.9	2.8 ± 1.4
101	ILE	-23.6 ± 2.5	-20.4 ± 9.5	137	VAL	-22.6 ± 2.6	-31.1 ± 4.3
102	SER	3.4 ± 1.0	2.1 ± 1.2	138	ASN	4.0 ± 1.0	1.9 ± 1.3
103	ALA	0.6 ± 0.2	0.5 ± 0.2	139	TYR	0.6 ± 0.1	0.6 ± 0.2
104	ALA	0.1 ± 0.0	0.1 ± 0.0	140	GLU	-0.8 ± 0.3	-1.6 ± 0.7
105	GLU	-65.4 ± 3.5	-100.7 ± 4.5	141	GLU	-65.8 ± 3.4	-99.9 ± 4.8
water		-10.7 ± 1.1	-46.8 ± 2.1	water		-9.5 ± 1.3	-32.3 ± 1.8
Total		-213.6 ± 8.0	-354.5 ± 14.0	Total		-250.6 ± 7.7	-416.4 ± 12.9

Table S3: Inter-fragment interaction energy (IFIE, average values of 100 structures, standard deviation, maximum value, and minimum value) of residue–residue pairs within Ca^{2+}–CaM and Eu^{3+}–CaM (unit in kcal·mol^{-1}).

		within N-lobe				within C-lobe			
		ave.	S.D.	max.	min.	ave.	S.D.	max.	min.
–/–	Ca	23.2	19.1	108.4	8.8	25.5	19.7	110.7	8.9
	Eu	24.2	22.8	123.5	9	27.1	24	124.2	7.9
–/+	Ca	-20.6	10.3	-9	-63.1	-24.6	20.3	-10.4	-126.4
	Eu	-19.6	9	-8.7	-54.7	-25.6	21.8	-10.6	-122.6
+/+	Ca	20.9	8.3	34	12.8	20.7	6.5	30.6	16.1
	Eu	20.1	7.7	30	12.4	21.3	8	34.2	14.3

		within α-helix				All			
		ave.	S.D.	max.	min.	ave.	S.D.	max.	min.
–/–	Ca	24	9	44.4	13.8	15	13.7	110.7	5.2
	Eu	23.8	7.8	35.8	14.9	15.5	15.8	124.2	5.3
–/+	Ca	-37.1	33.7	-10.6	-123.1	-15.5	14.3	-5.3	-126.4
	Eu	-36.1	31.8	-10.6	-132	-15.4	14	-5.5	-132
+/+	Ca	20.3	8.2	37.5	12.9	12.9	6.9	37.5	5.6
	Eu	19.8	7.6	33.5	12.2	13.1	6.6	34.2	5.8

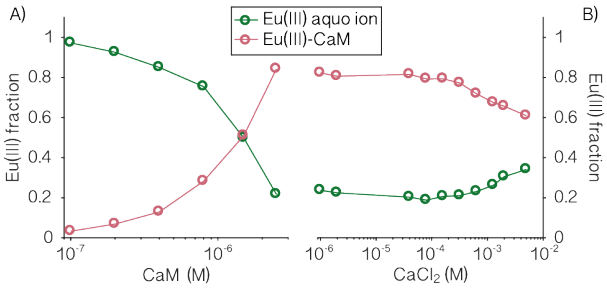

Figure S1: Calcium titration to Eu-CaM. Left: CaM was titrated to 10^{-5} M $EuCl_3$. At 2.5×10^{-5} M CaM roughly 80% of Eu(III) was bound to the protein. Right: Calcium titration to the Eu(III)-CaM complex. Even with 500 times excess of calcium over europium, the Eu^{3+}aquo ion fraction only increased from 20% to 34%.

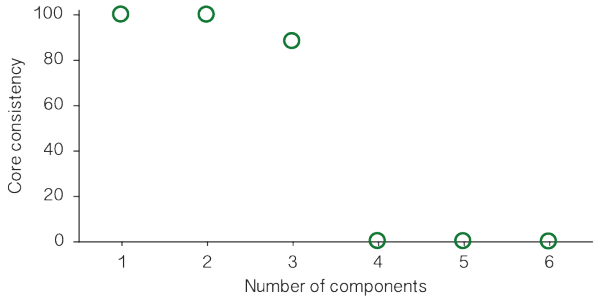

Figure S2: Core consistency for the analysis with different number of components. A valid number of components should have a high core consistency, close to 100.[7]

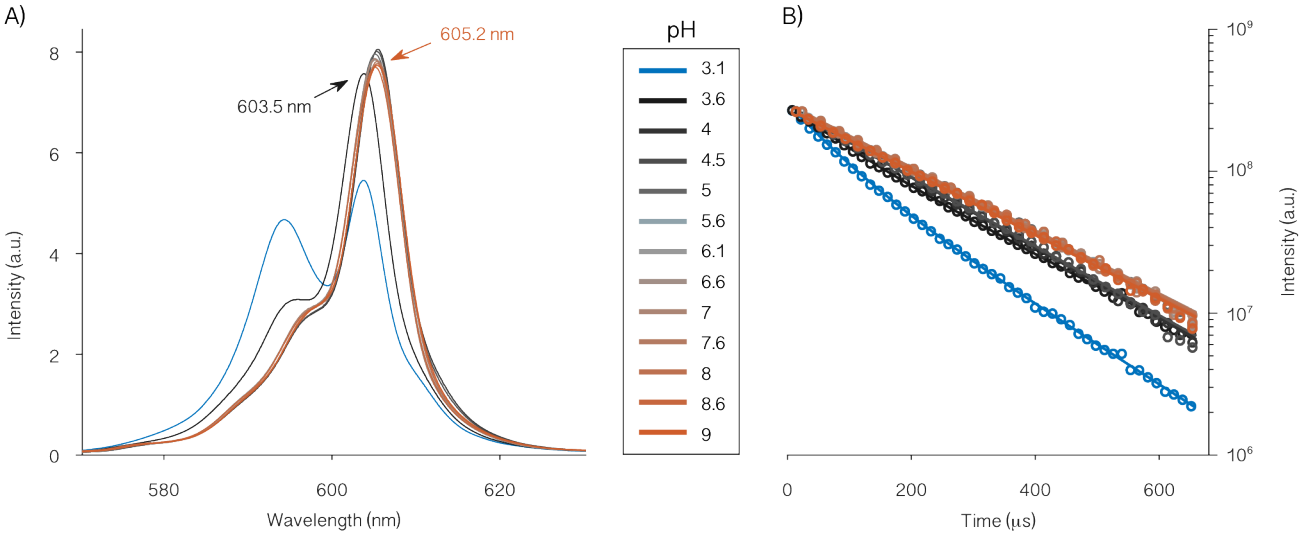

Figure S3: Complete set Cm^{3+}+ CaM. (A) Area-normalized Cm^{3+} luminescence emission spectra in the presence of CaM and (B) luminescence decay.

Table S4: Luminescence lifetimes observed in a Cm^{3+} + CaM mixture under variable pH extracted from integrated luminescence spectra.

pH	τ_1 (μs)	$n_1(H_2O)^a$	τ_2 (μs)	$n_2(H_2O)^a$
3.11	67.8 ± 3.8	8.7	156 ± 9	3.3
3.55	88.0 ± 24	6.5	199 ± 35	2.4
4.04	175 ± 2	2.8		
4.51	178 ± 2	2.8		
5.02	196 ± 2	2.4		
5.55	194 ± 2	2.5		
6.13	192 ± 2	2.5		
6.55	192 ± 3	2.5		
7.02	195 ± 1	2.4		
7.56	191 ± 3	2.5		
8.02	195 ± 2	2.5		
8.56	196 ± 2	2.4		
9.02	195 ± 2	2.5		

[a] The precision of the correlated number of water molecules n according to Kimura's equation is ± 0.5 H_2O.

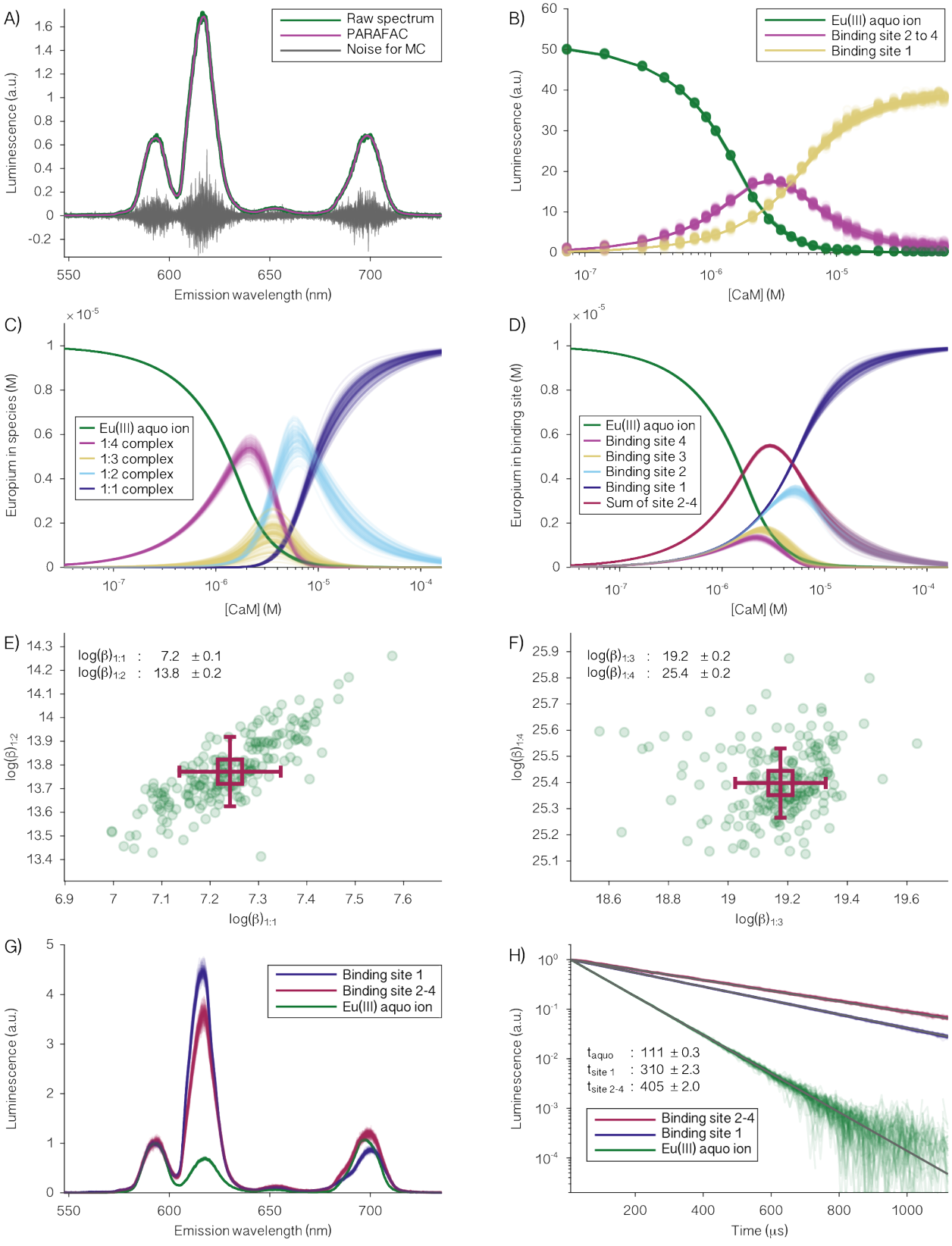

Figure S4: Monte Carlo error estimation of TRLFS for a series of 10 μM $EuCl_3$ and ~$7{\cdot}10^{-8}$ to ~$7{\cdot}10^{-5}$ CaM at pH 4.5. Plots showing the overlay of 200 MC runs (A) Raw spectrum and best fit PARAFAC spectrum (t=0 μs; sample $3{,}7{\cdot}10^{-6}$ M CaM). In gray is the random noise added for the MC runs. (B) PARAFAC deconvolution results. (C) Underlying speciation. (D) Contribution of each binding-site within the complexes; the 1:4 complex contained equal contributions of sites 1, 2, 3 and 4; the 1:3 complex contained equal contributions of sites 1, 2, and 3; the 1:2 complex contained equal contributions of sites 1 and 2; and the 1:1 complex only displayed a contribution form site 1. Assuming the same spectroscopic properties of site 2, 3 and 4, the contributions of these sites were summarized for the PARAFAC deconvolution. (E+F) Optimized log(β) including mean and standard deviation. (G) Luminescence emission spectra. H) Luminescence decays.

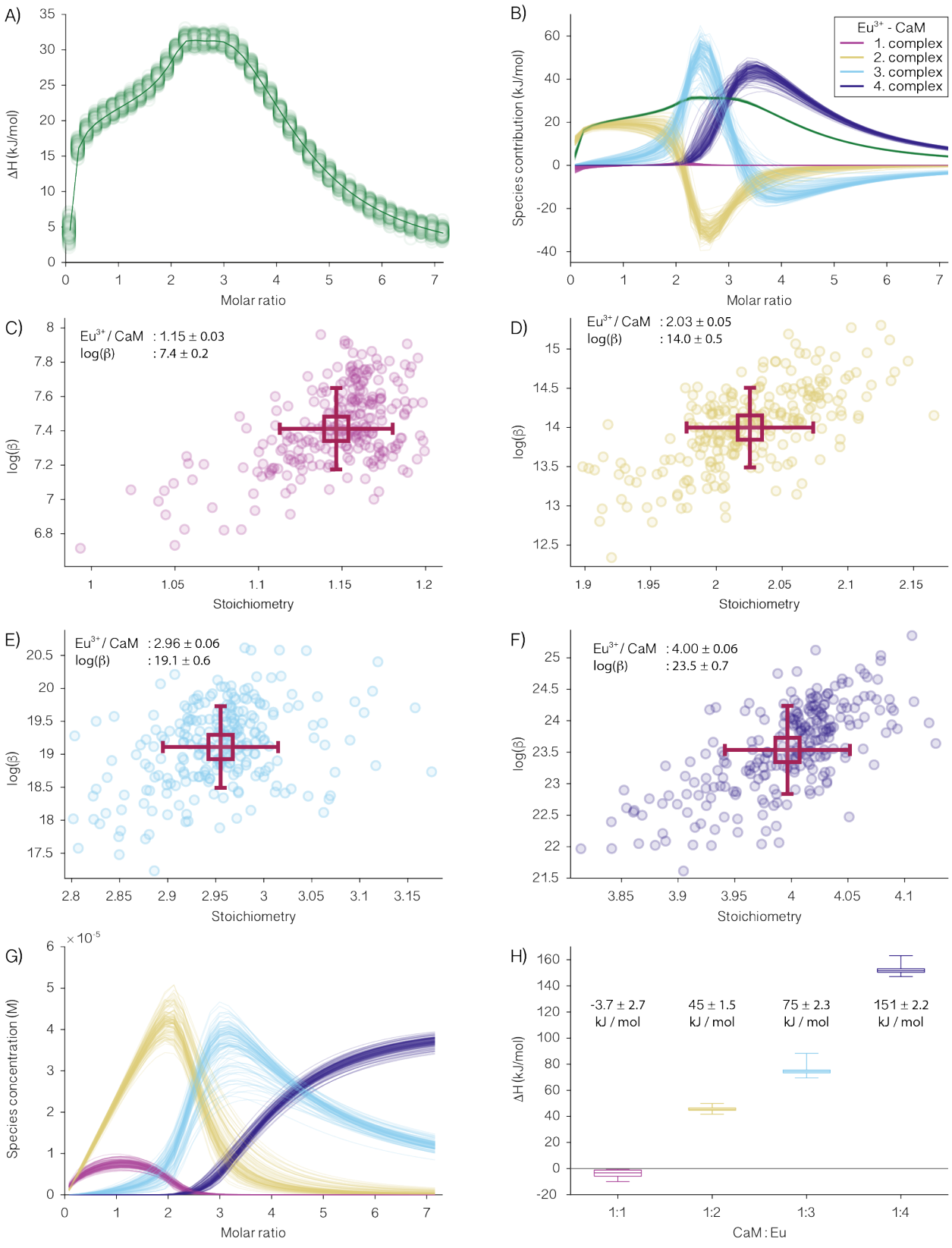

Figure S5: Monte Carlo error estimation of ITC of 2 mM $EuCl_3$ titrated to a 60 μM CaM solution at pH 4.5. Plots showing the overlay of 250 MC runs (A) Generated data for MC (symbols) compared to the best-fit of the data shown in the main text (line). (B) Fitted complex contributions to the measured heat. The sum of all complexes is shown in green. (C - F) Optimized log(β) versus complex stoichiometry, including mean and standard deviation (250 MC runs) for the 1:1 (C); 1:2 (D); 1:3 (E) and 1:4 (F) CaM-Eu(III) complexes. (G) Underlying speciation. (H) Boxplot of complex formation enthalpies of the four complexes.

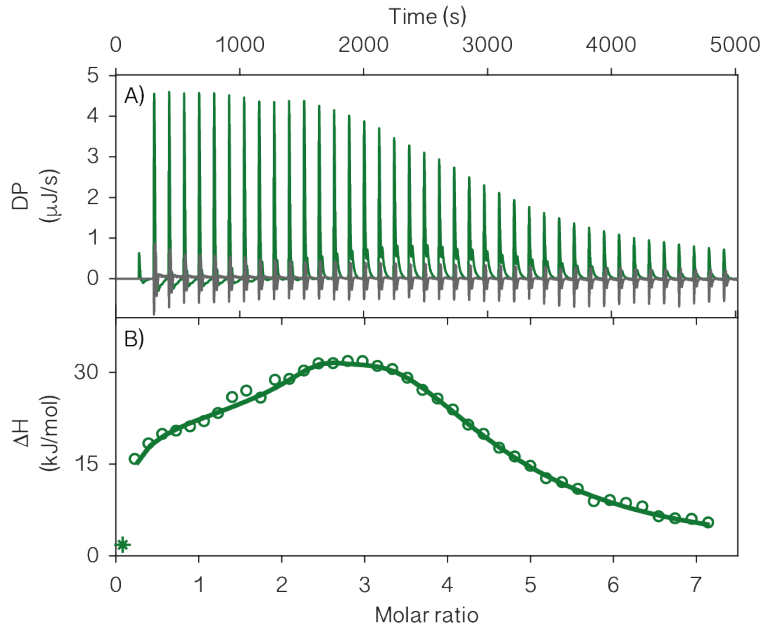

Figure S6: Replication of the ITC experiment from the main text. 2 mM $EuCl_3$ titrated to 60 μM CaM solution at pH 4.5

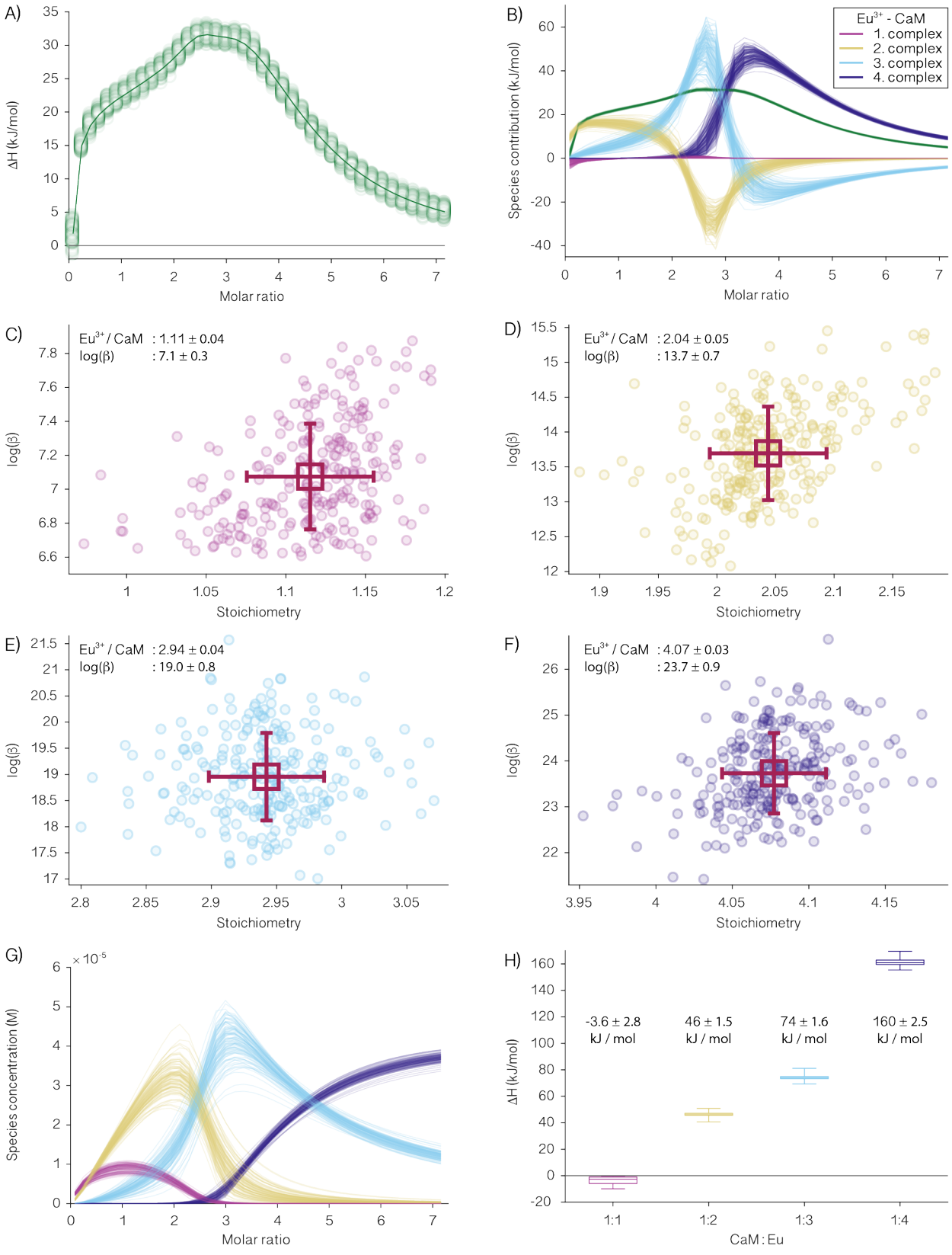

Figure S7: Monte Carlo error estimation of ITC replication of 2 mM $EuCl_3$ titrated to a 60 μM CaM solution at pH 4.5. Plots showing the overlay of 250 MC runs (A) Generated data for MC (symbols) compared to the best-fit of the data (SI Fig. S6; line). (B) Fitted complex contributions to the measured heat. The sum of all complexes is shown in green. (C - F) Optimized log(β) versus complex stoichiometry including mean and standard deviation (250 MC runs) for the 1:1 (C); 1:2 (D); 1:3 (E) and 1:4 (F) CaM-Eu(III) complexes. (G) Underlying speciation. (H) Boxplot of complex formation enthalpies of the four complexes.

Table S5: Kinetic parameters obtained for Ca^{2+}-CaM, enzyme alone, and enzyme in the presence of Eu^{3+}.

	PDE1 + Ca^{2+}-CaM	PDE1	PDE1 + Eu^{3+}-CaM
K_M (μM)	8.1 ± 0.2	20.3 ± 0.4	9.8 ± 0.3
k_{cat} (s^{-1})	14.0 ± 0.3	4.9 ± 0.1	11.9 ± 0.4

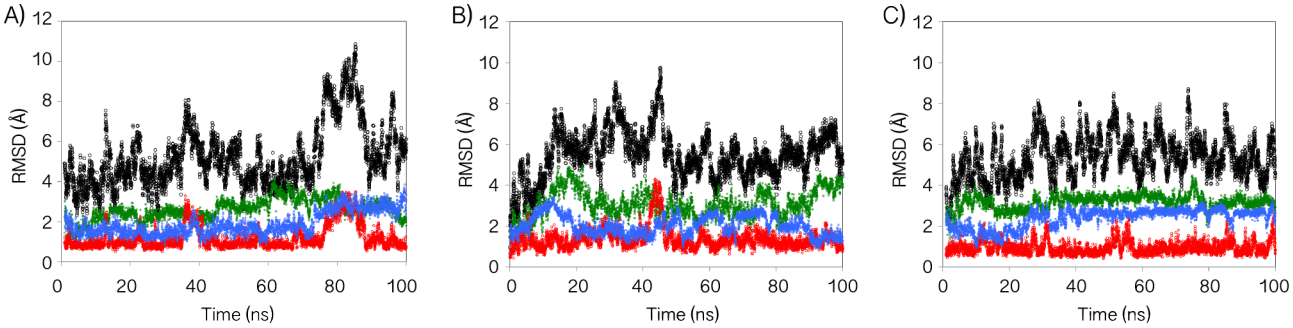

Figure S8: Time evolution of RMSD (for backbone atoms) of Ca^{2+}-(A), Eu^{3+}- (B), and Cm^{3+}-(C) bound CaM. Black: global structure, green: N-lobe, red: central helix, blue: C-lobe.

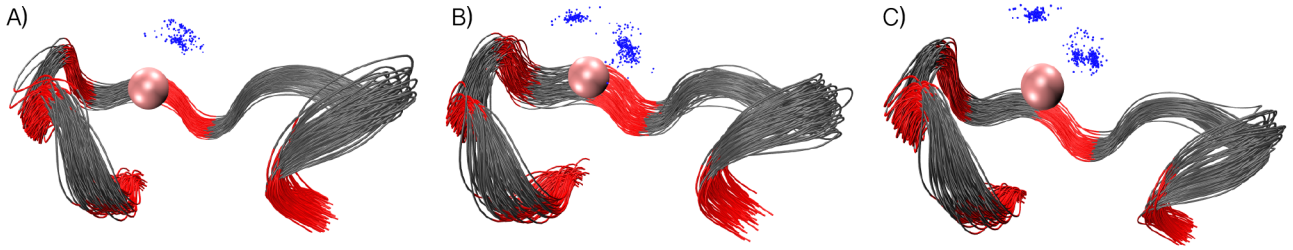

Figure S9: Superposition of 100 MD snapshots of EF–Hand 3 of Ca^{2+}– (A), Eu^{3+}– (B), and Cm^{3+}–(C) bound CaM. Pink balls represent metal ions, red and gray ribbons represent binding and non–binding residues, respectively, and blue dots indicate coordinating waters.

References

[1] Park, H. Y.; Kim, S. A.; Korlach, J.; Rhoades, E.; Kwok, L. W.; Zipfel, W. R.; Waxham, M. N.; Webb, W. W.; Pollack, L. Conformational changes of calmodulin upon Ca2+ binding studied with a microfluidic mixer. *Proceedings of the National Academy of Sciences* **2008**, *105*, 542–547.

[2] Olsen, S. N. Applications of isothermal titration calorimetry to measure enzyme kinetics and activity in complex solutions. *Thermochimica Acta* **2006**, *448*, 12–18.

[3] Todd, M. J.; Gomez, J. Enzyme kinetics determined using calorimetry: a general assay for enzyme activity? *Analytical biochemistry* **2001**, *296*, 179–187.

[4] Shannon, R. D. Revised effective ionic radii and systematic studies of interatomic distances in halides and chalcogenides. *Acta crystallographica section A: crystal physics, diffraction, theoretical and general crystallography* **1976**, *32*, 751–767.

[5] Ouyang, H.; Vogel, H. J. Metal ion binding to calmodulin: NMR and fluorescence studies. *Biometals* **1998**, *11*, 213–222.

[6] Kimura, T.; Choppin, G. R. Luminescence study on determination of the hydration number of Cm (III). *Journal of Alloys and Compounds* **1994**, *213*, 313–317.

[7] Andersson, C. A.; Bro, R. The N-way toolbox for MATLAB. *Chemometrics and intelligent laboratory systems* **2000**, *52*, 1–4.

[8] Drobot, B.; Steudtner, R.; Raff, J.; Geipel, G.; Brendler, V.; Tsushima, S. Combining luminescence spectroscopy, parallel factor analysis and quantum chemistry to reveal metal speciation–a case study of uranyl (VI) hydrolysis. *Chemical science* **2015**, *6*, 964–972.

[9] Drobot, B.; Bauer, A.; Steudtner, R.; Tsushima, S.; Bok, F.; Patzschke, M.; Raff, J.; Brendler, V. Speciation studies of metals in trace concentrations: the mononuclear uranyl (VI) hydroxo complexes. *Analytical chemistry* **2016**, *88*, 3548–3555.

[10] Case, D. A. et al. Amber 14. University of California, San Francisco, 2014.

[11] Bradbrook, G. M.; Gleichmann, T.; Harrop, S. J.; Habash, J.; Raftery, J.; Kalb, J.; Yariv, J.; Hillier, I. H.; Helliwell, J. R. X-Ray and molecular dynamics studies of concanavalin-A glucoside and mannoside complexes Relating structure to thermodynamics of binding. *Journal of the Chemical Society, Faraday Transactions* **1998**, *94*, 1603–1611.

[12] Baaden, M.; Berny, F.; Madic, C.; Wipff, G. M3+ lanthanide cation solvation by acetonitrile: The role of cation size, counterions, and polarization effects investigated by molecular dynamics and quantum mechanical simulations. *The Journal of Physical Chemistry A* **2000**, *104*, 7659–7671.

[13] Atta-Fynn, R.; Bylaska, E. J.; Schenter, G. K.; De Jong, W. A. Hydration shell structure and dynamics of curium (III) in aqueous solution: first principles and empirical studies. *The Journal of Physical Chemistry A* **2011**, *115*, 4665–4677.

[14] Komeiji, Y.; Ueno, Y.; Uebayasi, M. Molecular dynamics simulations revealed Ca2+-dependent conformational change of Calmodulin. *FEBS letters* **2002**, *521*, 133–139.

[15] Martyna, G. J.; Hughes, A.; Tuckerman, M. E. Molecular dynamics algorithms for path integrals at constant pressure. *The Journal of chemical physics* **1999**, *110*, 3275–3290.

[16] Komeij, Y.; Okiyama, Y.; Mochizuki, Y.; Fukuzawa, K. Explicit solvation of a single-stranded DNA, a binding protein, and their complex: a suitable protocol for fragment molecular orbital calculation. *Chem-Bio Informatics Journal* **2017**, *17*, 72–84.

[17] Amari, S.; Aizawa, M.; Zhang, J.; Fukuzawa, K.; Mochizuki, Y.; Iwasawa, Y.; Nakata, K.; Chuman, H.; Nakano, T. VISCANA: Visualized cluster analysis of protein- ligand interaction based on the ab initio fragment molecular orbital method for virtual ligand screening. *Journal of Chemical Information and modeling* **2006**, *46*, 221–230.